

Dynamic Properties of Magnesium Oxychloride-Titanium Gypsum Mineral Material after Freeze-thaw Cycles

Shuren WANG¹, Zihao SONG², Jian GONG^{3*}, Mintae KIM⁴ and Marcin RABE⁵

Authors' affiliations and addresses:

¹ School of Civil Engineering, Henan Polytechnic University, Jiaozuo 454003, China
e-mail: shurenwang@hpu.edu.cn

² School of Civil Engineering, Henan Polytechnic University, Jiaozuo 454003, China
e-mail: 920511830@qq.com

³ School of Civil Engineering, Henan Polytechnic University, Jiaozuo 454003, China
e-mail: gongjian@hpu.edu.cn

⁴ School of Civil, Environmental, and Architectural Engineering, Korea University, Seoul 02841, Republic of Korea
e-mail: kmt8262@gmail.com

⁵ Management Institute, University of Szczecin, Szczecin 70-453, Poland
e-mail: marcin.rabe@usz.edu.pl

*Correspondence:

Jian GONG, School of Civil Engineering, Henan Polytechnic University, Jiaozuo 454003, China
tel.: +86 13603448053
e-mail: gongjian@hpu.edu.cn

Funding information:

National Scholarship Fund of China [2023]-21, Key Project of Natural Science Foundation of Henan Province, China (232300421134), First-Class Discipline Implementation of Safety Science and Engineering (AQ20230103), and Zhongyuan Science and Technology Innovation Leading Talent Program (244200510005), China.

Acknowledgement:

The authors would like to express their sincere gratitude to the editor and reviewers for their valuable comments, which have greatly improved this paper.

How to cite this article:

Wang, S.R., Song, Z.H., Gong, J., Kim, M. and Rabe M. (2025). Dynamic properties of magnesium oxychloride-titanium gypsum composite material after freeze-thaw cycles. *Acta Montanistica Slovaca*, Volume 30 (1), 142-153

DOI:

<https://doi.org/10.46544/AMS.v30i1.11>

Abstract

Magnesium oxychloride cement (MOC)-based titanium gypsum (TG) composite material is a new type of green and energy-saving material. To reveal the uniaxial compressive strength and impact dynamic properties of MOC-TG composite material after multiple freeze-thaw cycles, an electromagnetic-driven Hopkinson bar impact test and a microcomputer-controlled electro-hydraulic servo universal testing machine were used to analyze the strength variation characteristics of MOC composite material with 30% TG after 0, 10, 20, 30, and 40 freeze-thaw cycles. Results show that with the increase in the number of freeze-thaw cycles, both the dynamic impact strength and uniaxial compressive strength of the MOC-TG composite material first increase and then decrease. The ductility of MOC is significantly improved after the addition of TG, and the MOC-TG composite material exhibits good frost resistance. The conclusions obtained in this study can provide a reference for improving the frost-thaw damage resistance of MOC-TG and its strength characteristics after multiple freeze-thaw cycles.

Keywords

Magnesium oxychloride cement, Titanium gypsum, Dynamic properties, Hopkinson bar, Freeze-thaw cycles.



© 2025 by the authors. Submitted for possible open access publication under the terms and conditions of the Creative Commons Attribution (CC BY) license (<http://creativecommons.org/licenses/by/4.0/>).

Introduction

Currently, the exploration of Magnesium oxychloride cement (MOC) has predominantly concentrated on material preparation processes, mechanical properties, and durability. MOC's mechanical performance and durability have been enhanced through adjustments in the Molar ratio and the incorporation of admixtures (Lauermannova et al., 2020; Rawat et al., 2024). Additionally, composite applications of MOC with other materials, such as the addition of fibre reinforcement and fillers, have been explored to elevate its overall performance. Globally, the focus of MOC research has extended to its performance in special environments and engineering applications. Studies have scrutinized the performance of MOC in harsh conditions like high and low temperatures, as well as acidic and alkaline environments, and its utilization in niche sectors like nuclear and marine engineering (Klunghirun et al., 2024).

Furthermore, investigations have delved into MOC's compatibility and interfacial reactions with other materials, aiming to improve its bonding strength and durability when combined. While significant progress has been made in MOC research on both domestic and international fronts, certain unresolved issues persist, including optimizing material preparation processes, augmentation of mechanical properties, and improving durability. With the escalation in military conflicts and the imperative to fortify the resistance to freeze-thaw cycles and dynamic impact strength of infrastructural entities such as airports, ports, docks, and various industrial and civil edifices, the assessment of the uniaxial compressive strength and impact dynamic characteristics of materials following numerous freeze-thaw cycles has acquired paramount importance (Solatiyan et al., 2024). The repetitive freezing and thawing of water within concrete can significantly compromise its mechanical properties, posing a significant risk to concrete structures and diminishing their service life (Donald et al., 2023). Hence, it is crucial to scrutinize the uniaxial compressive strength and impact dynamic attributes of concrete materials post-multiple freeze-thaw cycles.

As an eminent concern in the realm of solid waste management, titanium gypsum (TG) harbors a plethora of impurities and accumulates in substantial quantities (Gong et al., 2024; Wang et al., 2024a). Liaoning Province in China boasts abundant magnesite resources, furnishing ample raw materials for MOC manufacture. MOC, an eco-friendly cementitious substance, exhibits promising applications in road construction, bridge engineering, and architectural projects in sustainable development (Rodríguez-Alfaro et al., 2024; Lauermannová et al., 2024). The sulfuric acid process predominates in the production of titanium dioxide, where most of the acidic wastewater, after partial concentration and purification for reuse, is neutralized by adding alkaline substances such as limestone, lime, and carbide slag, resulting in the precipitation of gypsum ($\text{CaSO}_4 \cdot 2\text{H}_2\text{O}$), also known as TG (Hughes, 2010; Gázquez et al., 2021). The presence of TG solid waste not only takes up land space but also jeopardizes water sources and contributes to air pollution (Kim et al., 2016). Wang et al. (2024b) observed an initial surge followed by a decline in the compressive strength of MOC-TG with growing TG quantity, albeit with an improvement in ductility. In this study, the mechanical attributes of MOC-TG through additional freeze-thaw cycles were analyzed at a 30% TG dosage.

By substituting 30% MgO in MOC with fly ash, slag, a portion of kaolin, and calcined iron-rich kaolin, the water resistance of the cementing material can be bolstered (Aiken et al., 2022a). Ge et al. (2022), in their research on MOC additives, pointed out that citric acid significantly improved both the water resistance and strength of MOC. Experimental endeavors investigating diverse dosages and admixture ratios underscore the existing deficiencies in magnesium cement materials, particularly in terms of water resistance, necessitating further exploration (Aiken et al., 2022b). Furthermore, a mounting body of research is dedicated to the mechanical attributes of concrete after repeated freezing and thawing processes. Xu et al. (2024) investigated the damage mechanism in concrete samples subjected to low-stress impact fatigue loading following repeated freezing and thawing processes. Their study revealed that concrete endured more damage from freeze-thaw cycles than from low-stress impact fatigue (LIF) under short loading durations. However, notwithstanding these conditions, the impact of LIF loading on concrete damage was minimal, providing valuable insights into estimating concrete strength under compression post-freeze-thaw exposure.

In summary, recurrent freezing and thawing processes pose a formidable peril to concrete structures in cold regions, endangering lives and property. Nonetheless, scant research exists on the dynamic impact strength of MOC-TG cementitious composites post multiple freeze-thaw cycles. This study endeavors to scrutinize the uniaxial compressive strength and dynamic impact properties of MOC-TG composites after multiple freeze-thaw cycles, providing a reference for enhancing the freeze-thaw resilience of MOC-TG and understanding its strength characteristics after repeated freeze-thaw cycles.

Materials and methods

Test materials

Given the inherent heterogeneity in material attributes across geographical boundaries, the MOC used in the tests was sourced from a specialized establishment in Guangzhou City, China, renowned for its proficiency in magnesium product fabrication. The reactivity of MgO was assessed using the hydration technique to ensure a

minimum MgO concentration of 85%. Hexahydrate magnesium chloride was procured from a reputable chemical reagent provider in Tianjin, China, while TG was obtained from Henan Bailian Chemical Co., Ltd. in Jiaozuo City, China. The water used in the study was sourced from the municipal supply. The concrete mix proportions are presented in the following tables (Tabs. 1 and 2).

Tab. 1. Chemical composition of MOC-TG

Ingredients	MgO	MgCl ₂ ·6H ₂ O	H ₂ O	TG
Content [%]	41.51	25.59	20.44	12.45

Tab. 2. Chemical composition of TG

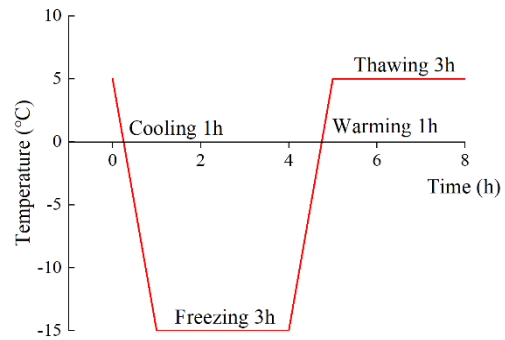
Ingredients	SO ₃	CaO	Fe ₂ O ₃	SiO ₂	Al ₂ O ₃	TiO ₂	MgO	Na ₂ O	MnO	Others
Content [%]	37.52	31.14	11.64	3.82	5.60	2.40	1.61	1.08	0.86	4.33

Elevated MgO content in the solution leads to increased alkalinity, thereby enhancing relative stability. However, it is crucial to maintain a MgO/MgCl₂ molar ratio below 6, as exceeding this threshold can have significant adverse effects on cement paste stability (Ba and Guan, 2009). To investigate how freeze-thaw iterations affect the compressive strength of cement made from magnesium chloride, a constant molar ratio of MOC (MgO:MgCl₂·6H₂O:H₂O) at 7:1:15 was employed. The quantity of TG is determined as a percentage of the mass of light-calcined magnesium oxide.

The MOC-TG solution, prepared according to specified proportions, was cast into cylindrical molds measuring Φ50 mm × 100 mm. After 24 hours, the samples are removed and cured under ambient conditions at 25°C (±5°C) for 28 days (Rahimi et al., 2023). Subsequently, the specimens were sections to dimensions of Φ50 mm × 25 mm and placed in a concrete rapid freeze-thaw cycling machine, model TDR-28, manufactured by Tianjin Gangyuan Test Instrument Factory. During the experiment, the temperature ranged from an upper limit of +5°C (±2°C) to a lower limit of -15°C (±2°C). Each cycle consists of a 4-hour cooling phase followed by a 4-hour heating phase, totaling 8 hours per cycle. After every two cycles, the specimens were maintained at 5°C for an additional 8 hours. This process facilitates the assessment of the impacts of varying freeze-thaw cycle counts on the TG-MOC composites (Fig. 1).



(a) Freeze-thaw testing machine



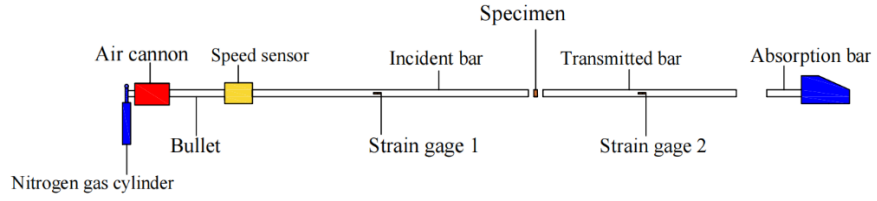
(b) Temperature history curve over time

Fig. 1. Rapid freeze-thaw testing machine and temperature history curve over time

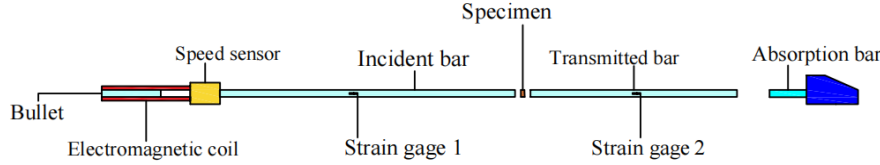
Experiment equipment

The dynamic impact experiments were conducted using the electromagnetic-driven Hopkinson bar (Fig. 2(b)) system. This approach harnesses electromagnetic driving technology to directly apply stress waves onto the incident bar through a secondary coil. In contrast, the conventional pneumatic Hopkinson bar (Fig. 2(a)) typically relies on compressed gas to propel a bullet that strikes the incident bar, thereby generating stress waves (Kamble and Tandaiya, 2024; Gong et al., 2022). The traditional pneumatic Hopkinson bar has undergone continuous improvements, evolving from uniaxial loading to concurrent multi-axial loading, such as triaxial or quadraxial loading, thereby allowing for a broader and more precise measurement range (Miyambo et al., 2023; Quillery et al., 2024).

The split Hopkinson pressure bar (SHPB) is a testing apparatus utilized to measure material properties at high strain rates. It comprises an electromagnetic drive, a bullet, an incident bar, and a transmission bar, all with a diameter of Φ50 mm. The incident bar of the SHPB, driven by electromagnetics, spans a length of 2.0 m, while the transmission bar measures 1.4 m in length, and the striker extends to 0.4 m. Both the incident and transmission bars are forged from pure steel with a chrome-plated surface to prevent corrosion (Fig. 3). For the static compressive strength tests, a universal testing machine manufactured by Zhongji Test Equipment Co., Ltd., with an electro-hydraulic servo control operated by a microcomputer of model YNS300, was utilized. This machine boasts a maximum testing force of 300 kN.



(a) Traditional pneumatic Hopkinson bar



(b) Electromagnetic drive Hopkinson bar

Fig. 2. Traditional pneumatic and electromagnetic drive Hopkinson bars

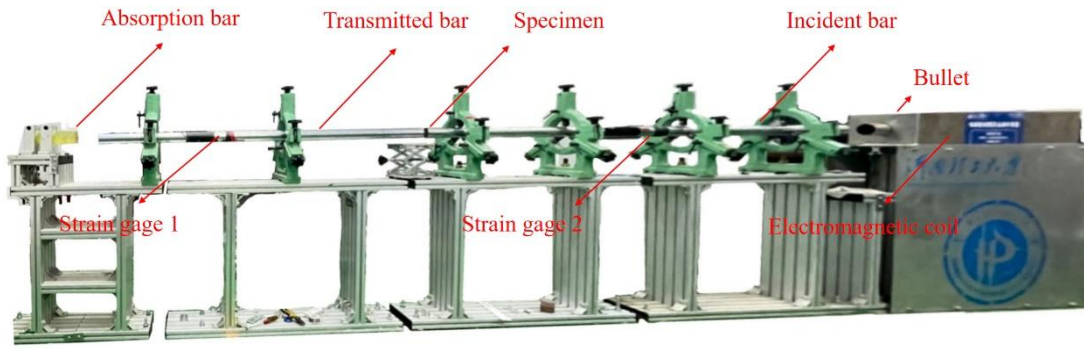


Fig. 3. Electromagnetic drive Hopkinson bar

Experimental process

Before the experiment commences, the incident, transmission, and absorption bars are aligned at the same horizontal level. The sample's cross-section is affixed to the incident bar's cross-section, with Vaseline applied to reduce the influence of friction on the experimental outcomes. Subsequent to positional adjustments and recalibration of the impact pressure, the striker impacts the incident bar, instigating pressure release that creates a stress wave within the cement along one dimension due to the variance in wave impedance between the magnesium oxychloride-based TG cement and the pressure bars. The collected data is then imported into the experimental data processing platform for subsequent analysis.

The voltage measured by strain gauges during testing can be leveraged to compute the mechanical parameters in the motion of MOC indirectly. The system subjects the specimen to dynamic impact at a high strain rate, with high-speed strain gauges on both sides to record incident and reflected waves and strain gauges on the transmission bar to capture the transmitted shock wave. The SHPB test employs the elastic stress wave theory and analyzes the data using the following three-wave method formulas. A dynamic stress-strain curve is constructed by analyzing the stress, strain, and strain rate recorded over the specimen's failure trajectory.

$$\sigma(t) = \frac{A}{2A_s} E(\varepsilon_i + \varepsilon_r + \varepsilon_t) \quad (1)$$

(2)

$$\varepsilon(t) = \frac{C}{l_s} \int_0^t (\varepsilon_i - \varepsilon_r - \varepsilon_t) dt \quad (3)$$

In the experimental setup, A , C , and E are used to denote the cross-sectional area, elastic wave velocity, and elastic modulus of the pressure bars, respectively. As represents the cement sample's cross-sectional area, while l_s denotes its length. The incident, reflected, and transmitted wave signals measured at time t are represented by ε_i , ε_r , and ε_t respectively. With these parameters, it is possible to derive the strain rate $\dot{\varepsilon}$, strain, and stress of the sample at time t .

According to the theory of elastic waves in one dimension, the pressures P_1 and P_2 , as well as the particle velocities V_1 and V_2 , can be obtained through the following procedures:

$$P_1(t) = A[\varepsilon_i(t) + \varepsilon_r(t)]E \quad (4)$$

$$(5)$$

$$P_2(t) = E\varepsilon_t(t)A \quad (6)$$

$$V_2(t) = C_0\varepsilon_t(t) \quad (7)$$

When $P_1=P_2$, it indicates that the specimen has reached a state of stress equilibrium.

$$\varepsilon_i(t) + \varepsilon_t(t) = \varepsilon_r(t) \quad (8)$$

Substituting Eq. (8) into Eqs. (1), (2), and (3), the calculation by the two-wave method unfolds:

$$\sigma(t) = \frac{AE}{A_s} \varepsilon_i(t) \quad (9)$$

$$\dot{\varepsilon}(t) = \frac{2C}{l_s} \varepsilon_t(t) \dot{\varepsilon}(t) = \frac{2C}{l_s} \varepsilon_t(t) \quad (10)$$

$$\varepsilon(t) = -\frac{2C}{l_s} \int_0^l \varepsilon_r(t) dt \quad (11)$$

The aforementioned equations underscore that with knowledge of the transmitted wave strain, elastic modulus, cross-sectional area, and other relevant parameters, it is viable to ascertain the axial pressure within the sample. Analyzing the strain values and strain rates makes it possible to calculate the specimen's instantaneous axial strain rate. According to the theory of elastic waves in one dimension, the strain gauge secured on the incident bar will capture the resulting shock wave when the bullet hits the incident bar. Upon impact, a segment of the incoming wave traverses the interface to the transmission bar and is detected by the strain gauge connected to it, known as the transmitted wave, while the residual wave rebounds, designated as a reflected wave.

To ensure the reliability of the dynamic mechanical testing results, the transmitted wave should be a combination of the incident and reflected waves in the shock process, which requires the stress equilibrium to reach a state similar to Fig. 4. This ensures a balanced distribution of stresses at both ends of the specimen, thereby minimizing the impact of inertial effects and allowing the specimen to respond to the applied stress wave primarily.

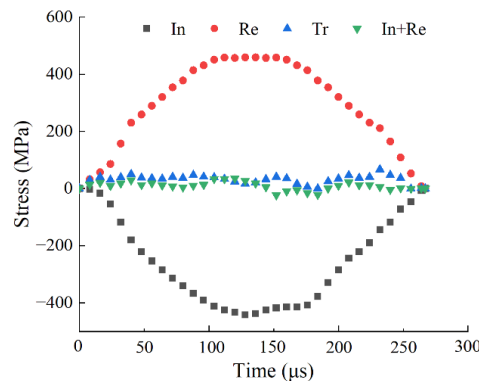


Fig. 4. Typical waveforms of the specimen

By utilizing a precision electronic balance with an accuracy of 0.01g, the weight differentials of the specimens pre and post each freeze-thaw cycle underwent meticulous measurement. Each set of specimens subjected to freeze-thaw cycles underwent weighing thrice for validation. Following multiple iterations of freezing and thawing, the specimen weights remained remarkably stable throughout the entire process, indicating that the recurrent freezing and thawing had negligible impact on the weight consistency of the specimens.

Before placement between the incident and the transmission bars, the test specimens were enveloped with white Vaseline on both of their end faces. Preceding the evaluations, a copper plate was affixed to the end face of the incident bar to ensure optimal electrical conductivity and signal transmission (Fig. 5).

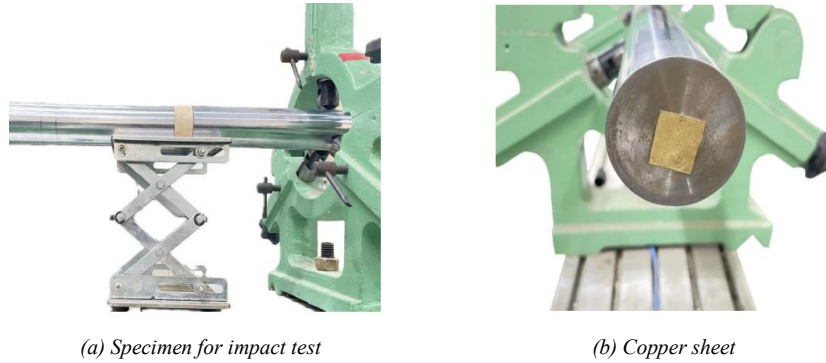


Fig. 5. Impact test sample and copper sheet

Upon 0, 10, 20, 30, and 40 cycles of repeated freezing and thawing, visual assessments of the specimens' conditions were recorded, following which both dynamic impact tests and static compressive tests were conducted. Dynamic impact tests were performed using an electromagnetic-propelled Hopkinson pressure bar at voltage levels of 1300 V (5.0 m/s), 1400 V (5.4 m/s), and 1500 V (5.8 m/s), with 15 specimens tested under each setting. Concurrently, static compressive tests were conducted using a universal testing machine, applying a loading rate of 0.5 kN/s to specimens corresponding to each freeze-thaw cycle count. Three specimens were scrutinized under each condition, and the mean results were derived from the amassed dataset.

Results analysis and discussion

Change characteristics of stress-strain curves

Brittle materials often exhibit an elevated dynamic critical load-bearing capacity (peak stress) under intensified strain rate impact loadings, a phenomenon recognized as the strain rate effect of brittle materials (Xi et al., 2024). Fig. 6 illustrates the relationships observed at varying impact speeds (5.0 m/s, 5.4 m/s, 5.8 m/s) and subsequent to iterative freezing and thawing processes (0, 10, 20, 30, 40 times).

The data depicted in Fig. 6 indicates that the maximum stress levels of cement, when subjected to freeze-thaw cycles, ascend proportionally with the escalation of strain rate, thereby demonstrating a conspicuous strain rate dependency. Additionally, the ultimate strain capacity of the material also escalates with higher strain rates. Broadly speaking, materials sensitive to strain rate show an upward trend in maximum stress levels with increasing strain rate while simultaneously encountering a decline in maximum strain level, a phenomenon commonly referred to as "dynamic embrittlement". However, cement materials, attributable to the abundance of microcracks and micropores as inherent flaws within their structure, manifest a combined interplay of strain rate hardening and damage softening (microdefect proliferation) under impact loading.

During the initial stages of loading, when the microdefects inherent in the cement have not undergone substantial expansion or proliferation, the material experiences a relatively minor impact, dominated by strain rate hardening. This instigates a rapid upsurge in stress levels with strain, thereby rendering the stress-strain curve predominantly linear. However, as the strain and stress intensify, the microcracks and micropores within the cement begin to expand and proliferate. Gradually, the cement absorbs more energy upon impact, leading to the propagation of microdefects and ultimately augmenting the ductility of the cement. Consequently, the stress-strain curve transitions into a convex nonlinear trajectory.

Comparatively, when subjected to high strain rates during the initial loading phases, a greater volume of microdefects is generated within the cement. This enhances the ductility of cement under high-speed loading scenarios. Furthermore, owing to the increased deformation rate, crack propagation circumvents the weakest interfaces in the material, initiating directly within their respective regions. Consequently, the material experiences increased peak stress and strain levels when exposed to high strain rate loading conditions.

To quantify the impact of strain rate on the material, the dynamic increase factor DIF is utilized to delineate the correlation between the strength during dynamic compression f_d and the static compressive strength f_c for the same freeze-thaw cycle count.

$$DIF = \frac{f_d}{f_c} \quad (12)$$

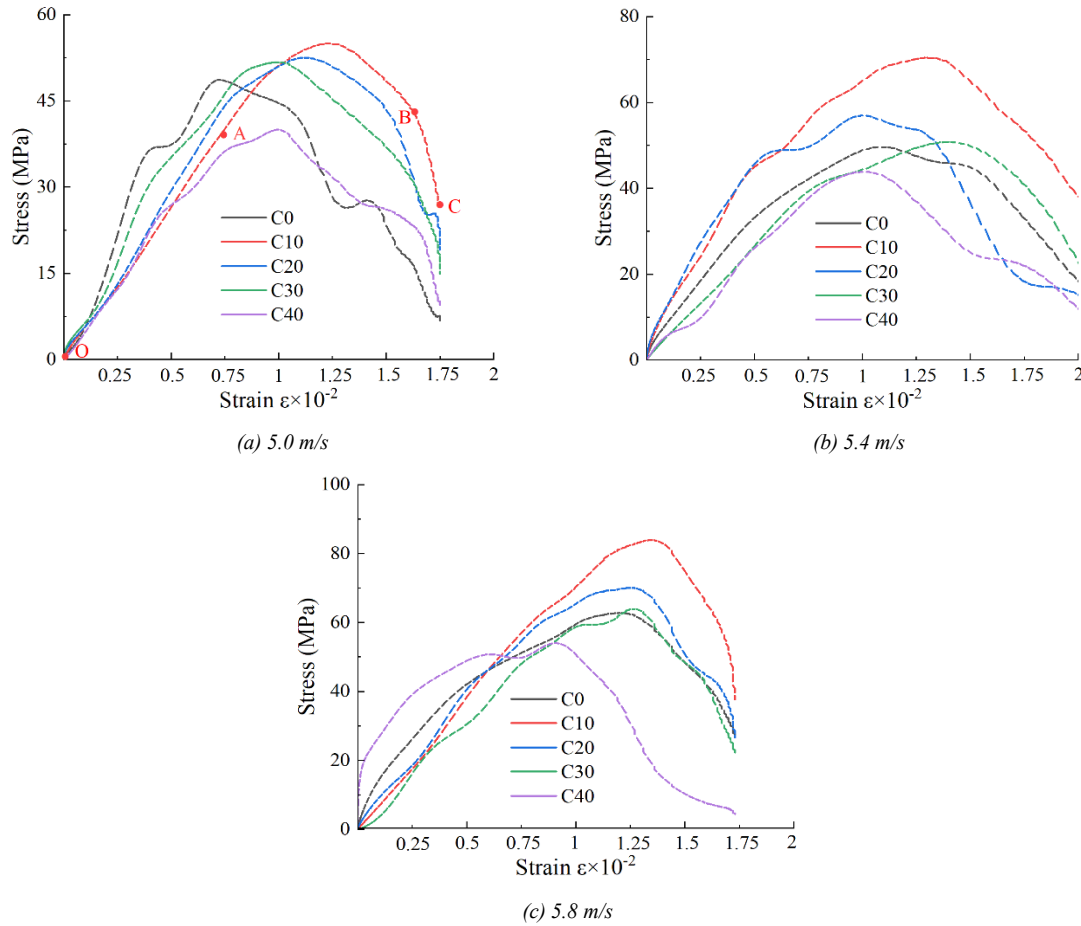


Fig. 6. Stress-strain graphs for MOC-TG under varying impact velocities

As demonstrated in Tab. 3, with constant freezing and thawing cycles, the *DIF* increases with elevated voltages.

Tab. 3. *DIF* of MOC-TG under different loading conditions

Name	C0	C10	C20	C30
$V=5.0$ m/s	1.04	1.14	1.20	1.21
$V=5.4$ m/s	1.06	1.46	1.30	1.19
$V=5.8$ m/s	1.34	1.74	1.60	1.50













The morphology of the TG-MOC samples noticeably evolves under impacts at different rates, with distinct failure modes characterized by blocky, flaky, and granular patterns. As observed in Tab. 4, the samples enduring 0 freezing and thawing processes are notably more fragmented than those exposed to 10 repeated freezing and thawing processes at various impact rates. Further, the extent of damage escalates progressively following 20, 30, and 40 cycles. Therefore, samples after 10 freeze-thaw cycles exhibit the least susceptibility to impacts across different rates compared to other control groups, indicating that the maximum strength of the samples is achieved after 10 freeze-thaw cycles.

The stress-strain curve of MOC during the dynamic impact test, as illustrated in Fig. 6, delineates three primary stages: elastic (OA), yield (AB), and failure (BC). Throughout the elastic phase, stress surges sharply as strain increases, approximating a linear trajectory. The impact load's energy is converted into elastic energy and stored within the sample. At this stage, the pores and cracks within the samples exhibit minimal development or interconnection, resulting in minimal impact on the samples. Subsequently, as the yield stage begins, stress peaks before declining with further strain, with the curve's slope initially decreasing and then increasing. During this phase, the specimens discharge the accumulated elastic energy. In the failure stage, the curve's slope increases once again, approximating a linear progression, and macroscopic fragmentation of the samples becomes evident.

With increasing cycles, the stress-strain graphs generally shift towards the lower right. Specifically, the tangent slope of the pre-peak ascending phase decreases, culminating in a reduction in deformation modulus and

peak stress, accompanied by an increase in peak strain and ultimate strain. When processing the waveform data using the three-wave method, it is observed that the general trend of the stress-strain curves remains stable regardless of variations in the striker's impact rates. However, the peak stress varies correspondingly, increasing with the loading rate (Fig. 6).

Tab. 4. Failure patterns of MOC-TG at different impact rates

Name	C0	C10	C20	C30
$V=5.0$ m/s				
$V=5.4$ m/s				
$V=5.8$ m/s				

Brittleness and ductility analysis of MOC-TG after freeze-thaw cycles

To investigate the brittleness and ductility of MOC-TG post-repeated freezing and thawing processes, its brittleness index B was characterized by the ratio of dynamic residual stress f_r to dynamic compressive strength f_d in impact tests.

$$B = \frac{f_r}{f_d} \quad (13)$$

According to Eq. (13), a smaller brittleness index signifies higher brittleness and lower ductility. The brittleness index under different freeze-thaw cycles is illustrated in Fig. 7.

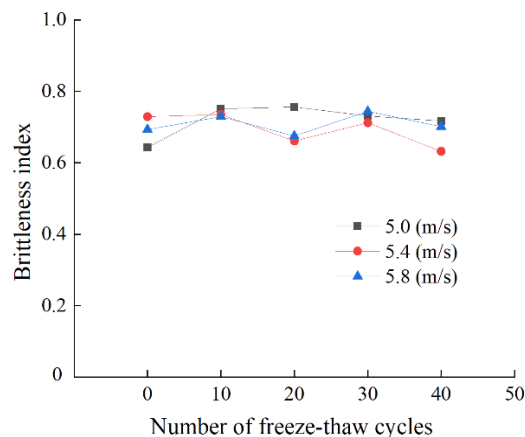


Fig. 7. Brittle-ductility diagram of MOC-TG

The trends observed in Fig. 7 make it clear that with more freezing and thawing processes applied, MOC-TG retains a notable level of ductility without displaying signs of brittleness damage resulting from the increased number of cycles. Therefore, subjecting MOC-TG samples to 0-40 freeze-thaw cycles does not compromise their ductility properties.

Dynamic elastic modulus analysis of MOC-TG after freeze-thaw cycles

The dynamic elastic modulus E_d , also known as the shear modulus, refers to the material's capacity to return to its original state post-deformation from a load. During impact, the stress-strain curve of the specimen typically traverses three stages: an initial elastic phase, followed by the yield phase, culminating in the failure stage. Therefore, the dynamic elastic modulus does not remain constant. In this study, E_d is defined as the secant modulus corresponding to 0.4 times the maximum stress in the initial segment of the stress-strain curve.

$$E_d = \frac{\sigma_{40}}{\varepsilon_{40}} \quad (14)$$

where, σ_{40} accounts for 40% of the maximum dynamic stress, while ε_{40} denotes the strain value corresponding to σ_{40} .

Fig. 8 illustrates the alterations in the dynamic elastic modulus of the sample under varying impact velocities, showcasing a gradual decline in its deformation resistance due to internal structural damage from repeated freeze-thaw cycles.

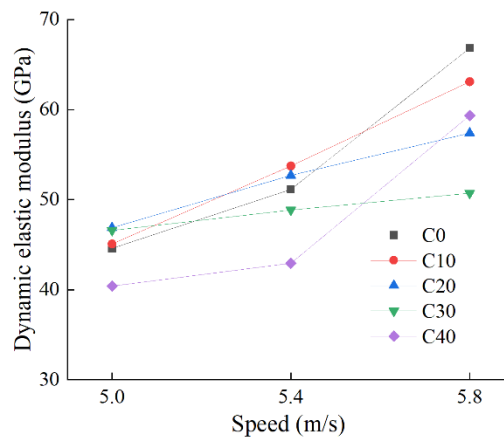


Fig. 8. Changes in dynamic elastic modulus of MOC-TG under different impact velocities

Variation characteristics of peak-stress

The data in Fig. 9 suggest an initial rise and subsequent drop in peak stress with varying cycle counts at various impact rates. Notably, specimens enduring 10, 20, and 30 freezing and thawing processes exhibit higher peak stress compared to those with 0 cycles. Results from dynamic impact tests across diverse impact rates have consistently confirmed the occurrence of the maximum strength after the 10th freeze-thaw cycle.

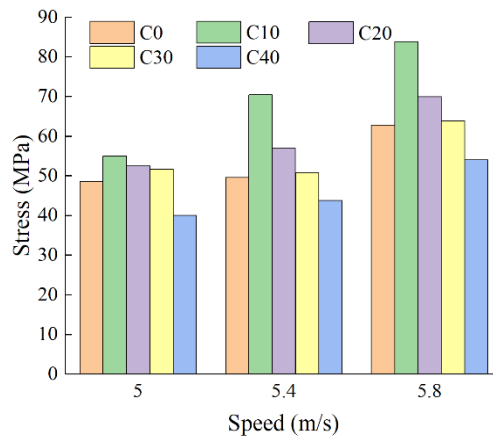


Fig. 9. Peak stress of MOC-TG under different impact rates

XRD analysis of MOC-TG after freeze-thaw cycles

The primary components of the MOC-TG composite include gypsum (CaSO_4), magnesite (MgO), hydrated lime ($\text{Ca}(\text{OH})_2$), and calcium titanium oxide (MgSiO_3). In the ternary system, the main hydration product is 5 ($5\text{Mg}(\text{OH})_2 \cdot \text{MgCl} \cdot 8\text{H}_2\text{O}$), with $\text{Mg}(\text{OH})_2$ emerging from incomplete phase 5 hydration.

Upon initial freeze-thaw cycles, the TG-MOC specimens undergo further reactions within their gel materials, leading to a heightened CaSO_4 and $5\text{Mg}(\text{OH})_2 \cdot \text{MgCl} \cdot 8\text{H}_2\text{O}$ contents, accompanied by a decrease in MgO content. This compositional enhancement results in an enhanced MOC-TG sample strength, peaking after the 10th freeze-thaw cycle. As cycle counts increase, CaSO_4 and $5\text{Mg}(\text{OH})_2 \cdot \text{MgCl} \cdot 8\text{H}_2\text{O}$ contents gradually diminish while MgO content rises, ultimately diminishing the MOC-TG material strength. This trend aligns with the observed variations in stress-strain behavior (Fig. 10).

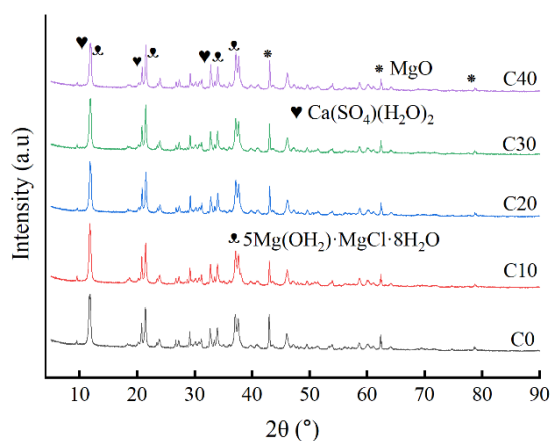


Fig. 10. XRD pattern of MOC-TG at different cycles

Conclusions

This study delves into the dynamic mechanical response and damage mechanisms of MOC-TG during alternating freezing and thawing processes through dynamic impact compression tests and static compressive tests. The analysis of impact velocities and repeated freezing and thawing processes sheds insights into the dynamic mechanical properties of MOC-TG. The main conclusions are obtained as follows:

(1) The TG-MOC cement specimens exhibit a catastrophic fragmentation failure mode under impact loading. With a boost in the impact velocity, the degree of fragmentation intensifies, characterized by an increased abundance of smaller fragments and finer powders. Conversely, the extent of fragmentation observed is minimally affected by the count of freeze-thaw iterations.

(2) The investigation reveals a direct augmentation of peak stress corresponding to the impact velocity of the bullet for a specific number of repeated freezing and thawing processes. Furthermore, as the impact velocity escalates, the differences in peak stress among specimens subjected to varying repeated freezing and thawing processes also widen.

(3) When the bullet's impact velocity remains constant, the strength of MOC-TG initially ascends and then descends with an increasing number of freezing and thawing iterations, peaking at 10 cycles before steadily declining. XRD analysis discloses the maximization of the phase 5 compound ($5\text{Mg}(\text{OH})_2 \cdot \text{MgCl} \cdot 8\text{H}_2\text{O}$) and calcium sulfate (CaSO_4) content after 10 cycles, contributing to the augmented strength of MOC-TG at this point.

Furthermore, this study underscores the imperative for further exploration into the water resistance of magnesium-based composites. Variations in moisture content have been identified as a pivotal factor that impacts the strength of MOC materials, necessitating additional research into the dynamic performance of TG-MOC cement after freeze-thaw cycling under different moisture conditions. Such investigations are supposed to furnish invaluable insights into optimizing the material for use in environments where water exposure and temperature fluctuations are prevalent.

Reference

Aiken, T. A., Kwasny, J., Russell, M., McPolin, D., Bagnall, L. (2022a). Effect of partial MgO replacement on the properties of magnesium oxychloride cement. *Cement and Concrete Composites*, 134, pp. 104791. DOI: 10.1016/j.cemconcomp.2022.104791.

- Aiken, T. A., Russell, M., McPolin, D., Gavin, B., Nugent, L., Bagnall, L. (2022b). Effect of molar ratios and curing conditions on the moisture resistance of magnesium oxychloride cement. *Journal of Materials in Civil Engineering*, 34(2), pp. 04021426. DOI: 10.1061/(ASCE)MT.1943-5533.0004070.
- Ba, H. J., Guan, H. (2009). Influence of MgO/MgCl₂ molar ratio on phase stability of magnesium oxychloride cement. *Journal of Wuhan University of Technology-Mater*, 24(3), pp. 476-481. DOI: 10.1007/s11595-009-3476-3.
- Donald, J., Monica, L., Robert, S., Peter, U., Elisabeth, H. (2023). Cementitious materials limitations for concrete exposed to deicing salt plus repeated cycles of freezing and thawing. *CE/papers*, 6(6), pp. 1168-1172. DOI: 10.1002/CEPA.2946.
- Gázquez, M. J., Contreras, M., PérezMoreno, S. M., Guerrero, J. L., CasasRuiz, M., Bolívar, J. P. (2021). A review of the commercial uses of sulphate minerals from the titanium dioxide pigment industry: the case of huelva (Spain). *Minerals*, 11(6), pp. 575. DOI: 10.3390/MIN11060575.
- Ge, M. L., Ye, Q. Q., Kang, H. J., Li, J. Z. (2022). Research progress of admixture-modified magnesium oxychloride cement. *Bulletin of the Chinese Ceramic Society*, 41(4), pp. 1202-1210. DOI: 10.16552/j.cnki.issn1001-1625.2022.04.028.
- Gong, J., Fang, D L., Liang, W. M., Wang, S. R. (2022). Influence factors analysis of projectile kinetic energy at muzzle of magnetoresistive coil gun. *Journal of Engineering Science and Technology Review*, 15(6), pp. 170-177. DOI: 10.25103/jestr.156.21.
- Gong, J., Zhang, J. X., Wang, S. R., He, M. C., Ma, A. C., Li, C. L. (2024). Experimental study on impact dynamic properties of magnesium oxychloride-doped paper sludge composites. *DYNA*, 99(5), pp. 531-537. DOI: <https://doi.org/10.52152/D11259>.
- Hughes, P. N., Glendinning, S., Manning, D. A. C., Noble, B. C. (2010). Production of "green" concrete using red gypsum and waste. *Proceedings of the Institution of Civil Engineers-Engineering Sustainability*, 163(3), pp. 137-146. DOI: 10.1680/ensu.2010.163.3.137.
- Kamble, A., Tandaiya, P. (2024). Modeling and simulation of dynamic compression of Bulk Metallic Glasses at room and elevated temperatures using split Hopkinson pressure bar setup. *International Journal of Plasticity*, 174, pp. 103915. DOI: 10.1016/J.IJPLAS.2024.103915.
- Kim, T. H., Tae, S. H., Chae, C. U., Choi, W. Y. (2016). The environmental impact and cost analysis of concrete mixing blast furnace slag containing titanium gypsum and sludge in south korea. *Sustainability*, 8(6), pp. 502. DOI: 10.3390/su8060502.
- Klungthirun, W., Theerapapvisetpong, A., Serivalsatit, K. (2024). Castable refractory materials from magnesium oxychloride cement-bonded cordierite-mullite. *Materials Letters*, 375, pp. 137217. DOI: 10.1016/J.MATLET.2024.137217
- Lauermannova, A. M., Antoncik, F., Lojka, M., Jankovsky, O., Pavlíková, M., Pivák, A., Záleská, M., Pavlík, Z. (2020). The impact of graphene and diatomite admixtures on the performance and properties of high-performance magnesium oxychloride cement composites. *Materials*, 13(24), pp. 5708. DOI: 10.3390/MA13245708.
- Lauermannová, A. M., Jankovsky, O., Jiricková, A., Záleská, M., Pivák, A., Pavlíková, M., Pavlík, Z. (2024). Recycling of magnesium oxychloride cement: Application of crushed MOC waste as a filler in the next-generation MOC composites. *Journal of Building Engineering*, 96, pp. 110499. DOI: 10.1016/J.JOBE.2024.110499.
- Lin, X., Liu, H. W., Zhou, Z. X., Liu, G. G., Ni, B. J., Wang, C. Q. (2024). Killing three birds with one stone: A novel valorization strategy for comprehensive utilization of waste titanium gypsum. *Construction and Building Materials*, 442, pp. 137680. DOI: 10.1016/J.CONBUILDMAT.2024.137680.
- Miyambo, M. E., Von, K. D. V., Pandelani, T., Reinecke, J. D. (2023). Review of the development of the split Hopkinson pressure bar. *Procedia CIRP*, 119, pp. 800-808. DOI: 10.1016/J.PROCIR.2023.04.010.
- Quillery, P., Durand, B., Huang, M., Seck, K., Zhao, H. (2024). Dynamic biaxial compression tests using 4 symmetric input hopkinson bars. *Experimental Mechanics*, 64(5), pp. 729-743. DOI: 10.1007/S11340-024-01056-Y.
- Rahimi, M. Z., Zhao, R. G., Sadozai, S., Zhu, F., Ji, N., Xu, L. P. (2023). Research on the influence of curing strategies on the compressive strength and hardening behaviour of concrete prepared with ordinary portland cement. *Case Studies in Construction Materials*, 18, pp. e02045. DOI: 10.1016/J.CSCM.2023.E02045.
- Rawat, S., Saliba, P., Estephan, P. C., Ahmad, F., Zhang, Y. X. (2024). Mechanical performance of hybrid fibre reinforced magnesium oxychloride cement-based composites at ambient and elevated temperature. *Buildings*, 14(1), pp. 270. DOI: 10.3390/BUILDINGS14010270.
- Rodríguez-Alfaro, L. F., Torres-Martínez, L. M., Treviño-Garzo, M. Z., Vázquez-Guillén, J. M., Rodríguez-Padilla, C., Luévano-Hipólito, E. (2024). Design and fabrication of photocatalytic magnesium oxychloride cement with improved moisture stability: A step towards sustainable construction. *Construction and Building Materials*, 414, pp. 134804. DOI: 10.1016/J.CONBUILDMAT.2023.134804.

- Solatiyan, E., Ibrahim, M. S., Vaillancourt, M., Carter, A. (2024). The mechanical performance of reinforced bituminous interfaces with paving fabric under freeze-thaw conditioning. *Construction and Building Materials*, 435, pp. 136809. DOI: 10.1016/J.CONBUILDMAT.2024.136809.
- Wang, S. R., Wang, Y., Gong, J., Zhao, L. R. (2024a). Water temperature change on performance of magnesium oxysulfate-based yellow gypsum foamed concrete. *Journal of Engineering Science and Technology Review*, 17(4), pp. 9-15. DOI: 10.25103/jestr.174.02.
- Wang, S. R., Zhao, L. R., Gong, J., Marcin, L., Wang, Y., Li, C. L. (2024b). Experimental research on mechanical properties of magnesium oxychloride-based titanium gypsum concrete. *DYNA*, 99(2), pp. 215-220. DOI: 10.6036/11171.
- Xi, Y. H., Dui, G. S., Sun, Z. Y., Dianen W. (2024). Strain-rate effect on mechanical properties of rock-like specimens with narrow crack under uniaxial compression. *Theoretical and Applied Fracture Mechanics*, 133, pp. 104542. DOI: 10.1016/J.TAFMEC.2024.104542.
- Xu, Y. Q., Yuan, Q., De, S. G., Xiang, G. K., Hu, C. L., Chen, L. (2024). Mechanism of concrete damage under the coupled action of freeze-thaw cycle and low-stress impact fatigue load: From pore structure to energy dissipation. *Construction and Building Materials*, 436, pp. 136980. DOI: 10.1016/J.CONBUILDMAT.2024.136980.